Prototype of a tensegrity manipulator to mimic bird necks

Matthieu Furet[a], Damien Chablat[a], Benjamin Fasquelle[a], Parag Khanna[b], Christine Chevallereau[a], Philippe Wenger[a]

a. Laboratoire des Sciences du Numerique de Nantes, CNRS, Ecole Centrale de Nantes, France, firstname.name@ls2n.fr

b. Ecole Centrale de Nantes, France, firstname.name@eleves.ec-nantes.fr

Résumé :

Une structure de tenségrité est un assemblage d'éléments en compression (barres) et d'éléments en traction (câbles, ressorts) maintenus ensemble en équilibre [1],[2]. La tenségrité est connue en architecture et en art depuis plus d'un siècle [3] et est adaptée à la modélisation des organismes vivants [4]. Les mécanismes de tenségrité ont été étudiés plus récemment pour leurs propriétés prometteuses en robotique telles que la faible inertie, la souplesse naturelle et la capacité de déploiement [5]. Un mécanisme de tenségrité est obtenu lorsqu'un ou plusieurs éléments sont actionnés. Ces travaux s'inscrivent dans le cadre du projet AVINECK, auquel participent des biologistes et des roboticiens dans le but principal de modéliser et de concevoir des cous d'oiseaux. En conséquence, une classe de manipulateurs de tenségrité planaire composée d'un assemblage en série de plusieurs mécanismes en X de Snelson [6], c'est-à-dire des mécanismes à quatre barres croisées avec des ressorts sur leurs côtés latéraux, a été choisie comme candidat approprié pour un modèle préliminaire plan d'un cou d'oiseau.

Le prototype consiste en un mecanisme en X de Snelson. Les barres sont assemblées selon différents plans pour éviter les collisions internes. Le manipulateur est entraîné par des câbles parallèles aux ressorts et traversant les axes grâce à des perçages. Chaque câble est attaché à un tambour. Le manipulateur est actionné par deux câbles, ce qui en fait un mécanisme antagoniste, dont on peut contrôler la raideur.

Les pièces structurelles (barres, supports, tambours) sont imprimées en 3D en ABS. Chaque liaison pivot entre les barres et les axes est construite avec deux roulements qui assurent un centrage long, et toutes les pièces sont arrêtées axialement avec des colliers d'arbre. Nous avons décidé d'avoir une longueur de barre transversale de 100 mm et une longueur de barre supérieure de 50 mm. Ces dimensions sont adaptées à plusieurs jeux de ressorts disponibles, c'est-à-dire que les ressorts considérés sont toujours en tension et ne sont pas trop étendus pour toutes les positions accessibles du manipulateur. Une fois la longueur et la raideur du ressort définies, le modèle statique est calculé afin d'obtenir la force d'entrée maximale pour les câbles. Cette force doit être suffisante pour actionner le mécanisme dans un grand espace de travail et pour résister aux chargements externes. La force appliquée par les câbles est directement liée au rayon du tambour et au couple du moteur. Le rayon du tambour influe également sur la vitesse de translation du câble. Un compromis est fait pour avoir des efforts et vitesses de câbles suffisants.

Deux variateurs interagissent avec un microprocesseur sur lequel est programmé la loi de commande. Chaque moteur est équipé d'un codeur pour connaître la position réelle du mécanisme. Le bon comportement du mécanisme est assuré par une commande dynamique.

Abstract :

This paper deals with the building of a 2D tensegrity mechanism. The considered mechanism is derived from the Snelson's X-shape mechanism and is used as an elementary part of the bird neck modelling. Indeed, an n-dof manipulator can be obtained by stacking in series n X-shape mechanisms. This paper explains the design and building process of a 1-dof prototype, both on hardware and software aspects, and will be used further to have experimental results on the dynamic modelling, control laws and actuation strategy.

Keywords : Tensegrity, Robotics, Bio-inspired design, Dynamics

1 Introduction

As birds do not have arms, they use their necks as manipulator for a whole set of tasks (feeding, cleaning, hanging, hammering,etc.). The bird necks presents amazing dexterity, dynamic performances, and can be a very good source of inspiration for robotic manipulators. The AVINECK project, involving both biologists and roboticists, aims at building a manipulator that mimics a bird neck. To link both disciplines, the concept of tensegrity has been chosen, as it is suited to model musculo-skeletal systems, and is also a very good candidate to build light-weight, deformable, high-performance robots. A tensegrity structure is a stable assembly of tensile elements (bars) and compressive elements (cables, springs)[2], [6]. Its use in robotics is quite recent [5],[7], [8], [9], [10], [11], [12], [13]. For this project, the modelling of a bird neck in 2D is done by stacking simple Snelson-X-shape mechanisms [6], which is composed of two rigid bars connected with tendons (springs and or cables). By modifying the cable tension, the equilibrium of the mechanism can be controlled. The modeling of such a mechanism has been done in previous work [14],[15], [16], [17]. This paper focuses on the practical building of a tensegrity prototype composed of one X-shape mechanism. The modelling of the mechanism is first introduced, then the practical aspects of this work are presented. Indeed, as this mechanism can have high dynamics, all parameters (geometric, mass and inertia, forces) needs to be taken into account and chosen with care. The control of the mechanism is implemented in a microchip that interacts with the motors directly. The building of this prototype is a first step to further work. First, the previous results obtained for the modelling of one X-shape mechanism will be experimentally validated. Then, starting from the same prototype base (motors, electronics), the stacking of several mechanisms can be done.

2 Mechanism modelling

An elementary X-shape tensegrity mechanism consists of a four-bar mechanism with crossed links and two pre-tensioned springs, which makes it a class 2 tensegrity mechanism. The links are considered rigid, homogeneous and linear and are built such that they are not subject to buckling. They are connected by A, B, C and D, which are assumed to be perfect revolute joints with no friction and damping, see Fig. 1. The mechanism is fixed to the ground by A and B. The two springs connect A and D, and B and C, and are considered massless. The mechanism data are given in Tab. 1. The two crossed links have the same length L and the base and top links have the same length b.

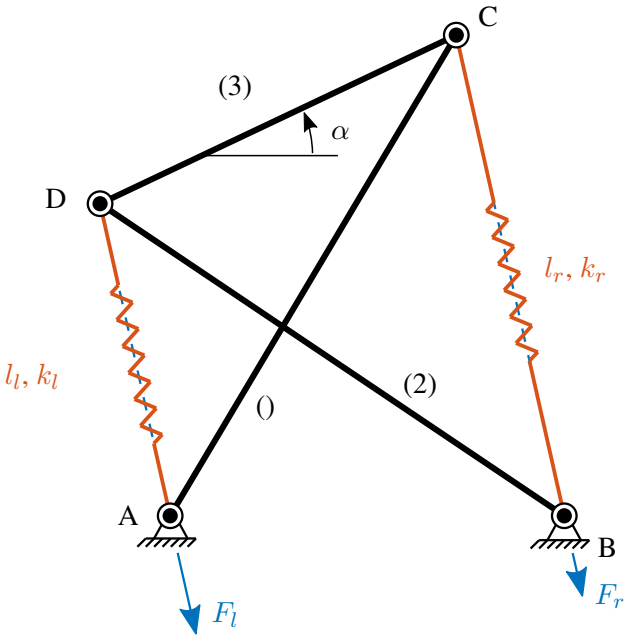

FIGURE 1 – Single module.

	Length	Mass	Stiffness
Link 1	b	m_1	-
Link 2	L	m_2	-
Link 3	L	m_3	-
Spring 1	l_1	-	k_1
Spring 2	l_2	-	k_2

TABLE 1 – Mechanism data.

The mechanism is actuated by tendons connected at hinges D and C and run through the springs and applied forces F_l and F_r, that are bounded by F_{max} and F_{min} and since tendons cannot push, F_{min} is positive. The rotation range of the mechanism is $-\pi < \alpha < \pi$, i.e. the mechanism cannot reach the flat singular configurations (possible in theory but difficult to achieve in practice due to collisions). The equation of motion has been derived in previous paper [18] thanks to the Lagrangian equation which is written in the following form :

$$M(\alpha)\ddot{\alpha} + C(\alpha)\dot{\alpha}^2 + G(\alpha) = Z_l(\alpha)F_l + Z_r(\alpha)F_r \tag{1}$$

where M is the mass and inertia term, C the term of coriolis effects and G the term of potential effects (springs and mass). Z_r and Z_l corresponds to the lever arm length of forces F_r and F_l with respect to the instantaneous center of rotation of the top bar (i.e the intersection point of the two crossed bars).

The static equilibrium condition is obtained if the velocities and accelerations are neglicted in equation (1) and F_l and F_r are considered as constant, which yields :

$$G(\alpha) = Z_r(\alpha)F_r + Z_l(\alpha)F_l \tag{2}$$

The right-hand side of equation (2) is the actuation wrench. The wrench feasible workspace (WFW) must respect, by definition, the kinematic constraint equations, the static equilibrium (equation (2)) and the limits for the external forces F_{max} and F_{min}. Accordingly, it is possible to determine the limits of the external wrench based on the limits of the external forces as follows :

$$\begin{aligned} \Gamma_{max}(\alpha) &= Z_l(\alpha)F_{max} + Z_r(\alpha)F_{min} \\ \Gamma_{min}(\alpha) &= Z_l(\alpha)F_{min} + Z_r(\alpha)F_{max} \end{aligned} \tag{3}$$

The external wrench is bounded by equation (3). Static equilibrium (equation (2)) is obtained for a range

Spring	Stiffness	free length l_0	max length l_{max}
1	$90\,N/m$	$0.037\,m$	$0.165\,m$
2	$130\,N/m$	$0.052\,m$	$0.191\,m$
3	$150\,N/m$	$0.047\,m$	$0.152\,m$
4	$190\,N/m$	$0.051\,m$	$0.152\,m$

TABLE 2 – Parameters of the different springs available

of α where G is within the feasible wrench bounding curves :

$$\Gamma_{min}(\alpha) \leq G(\alpha) \leq \Gamma_{max}(\alpha) \tag{4}$$

A control law is deduced from the dynamic model, where the Coriolis effects are neglected. For a desired trajectory $(\ddot{\alpha}_d, \dot{\alpha}_d, \alpha_d)$, the forces are computed such that

$$M(\alpha)\Big(\ddot{\alpha}_d + k_v(\dot{\alpha}_d - \dot{\alpha}) + k_p(\alpha_d - \alpha)\Big) + G(\alpha) = Z_l(\alpha)F_l + Z_r(\alpha)F_r \tag{5}$$

where k_p and k_v are the gains. There are infinite number of solutions for this equation, and a solution that minimizes the sum of the forces is chosen (bearing in mind that the two forces must be positive).

3 Prototyping

3.1 Requirements and dimensions

The dimensions of the prototype must first respect the kinematic constraint which imposes $L > b$. For this mechanism, the minimal length of the spring is given by $(L-b)$ and the maximal length by $(L+b)$, which corresponds to the flat configuration of the mechanism. From a large set of springs available in the lab (given in table 2), the best dimensions have been determined. The parameters L and b are chosen such that the maximal number of different springs available can be mounted on the prototype, allowing different behavior of the mechanism, non-symmetric spring stiffness, etc. We ensured that for each spring available, the free length l_0 was lower than $(L-b)$ and that the maximal stretched length of the spring l_{max} was higher than $(L+b)$. From that analysis, the dimensions for L and b has been chosen such that $L = 100\,mm$ and $b = 50\,mm$.

The two chosen motors are two MAXON brushless gearmotor (ECMAX40L/PM42). The datasheets of the motors are given in Tab. 3. The cables are attached to the motor shaft thanks to a drum, whose radius needs to be determined. In fact, the radius of the drum links the motor torque to the tension as well as the motor speed and cable speed. Thus, a radius of $20\,mm$ has been chosen for the drum, which gives a nominal tension of $155\,N$, taken as F_{max} and a nominal speed of $0.33\,m/s$ for the cables. With the previous computation of the geometric dimensions and spring stiffness available, the nominal force $F_{min} = 0\,N$, $F_{max} = 155\,N$ allows the prototype to reach almost the full range of the workspace as shown on figure 2 (flat configuration is avoided), and the nominal speed permits to go from one extreme position to an other in less than $0.5\,s$.

3.2 Mechanical assembly

A first design has been made with CAD software (3DEXPERIENCE), that highlighted the necessity to use different layers, in order to avoid collisions between bars. Each revolute joint is made around a shaft

Voltage	$24\,VCC$
Nominal current	$4\,A$
No load speed	$202\,rpm$
Nominal Torque	$3.10\,Nm$
Nominal speed	$160\,rpm$

TABLE 3 – Motor data of the motor ECMAX40L/PM42

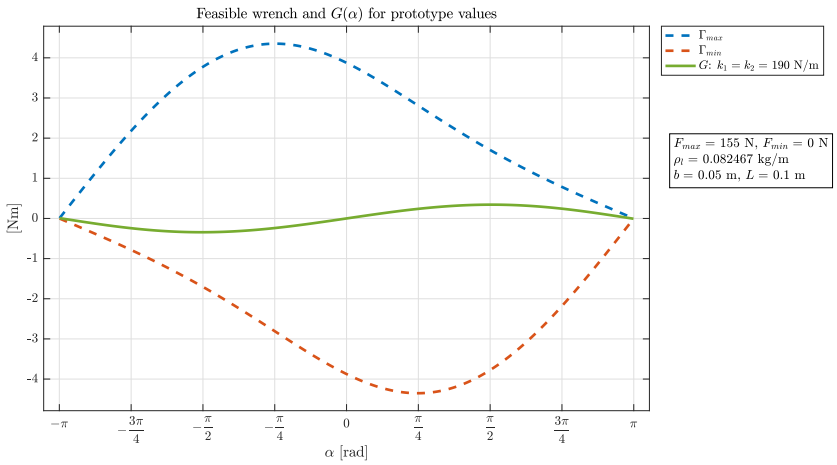

FIGURE 2 – Graph showing the maximal and minimal torque and the potential function G for the prototype parameters. All the positions α where $G(\alpha)$ is inside the space bounded by Γ_{min} and Γ_{max} are inside the Wrench feasible workspace

that links the bars with each other. Each bar has been 3D-printed in ABS. The revolute joint between the extremity of each bar and the shaft is ensured with two bearings. In fact, as the depth is used, two bearings ensuring long centering is better than only one bearing which allows swiveling and deformation of the prototype. Thus, two crossed bars are attached to the base of the mechanism, and two top bars for the link 3, in order to have more rigidity (see figure 3). Between the top-left and bottom-left shaft (respectively right), the left spring (resp. right) is attached and pre-tensioned, thus ensuring a stable equilibrium position of the mechanism (see figure 4). In the middle of each shaft, a small hole is made. The left cable (resp. right) is attached to the hole of the top shaft, then goes through the hole of bottom shaft. A last shaft is used as a pulley to reduce friction of the cable passing through the hole, and the cable is finally winded and attached to the drum. The drum is also 3D-printed and a screw ensures the proper winding of the cable around it.

3.3 Interfacing and algorithm

A Beaglebone (BB) blue microcontroller is used to control the prototype. This microcontroller offers a large set of functions and pins, from ADC to PWM and encoders inputs. Each MAXON motor is controlled thanks to an ESCON 50/5 controller, that ensures speed and torque control of each motor. ESCON controllers allows a direct linking from the encoder that measures the angular position of the motor, such that an internal speed control law is possible. In our case, we used a more complex control law involving dynamics, that is why we needed a micro-computer and an interface between encoders, the micro-computer and the controller (see figure 6.

The closed loop is presented on the Figure 5. Given a desired trajectory $(\ddot{\alpha}_d, \dot{\alpha}_d, \alpha_d)$ and the current position α, the forces to be applied are computed with the dynamic control law provided in equation (5).

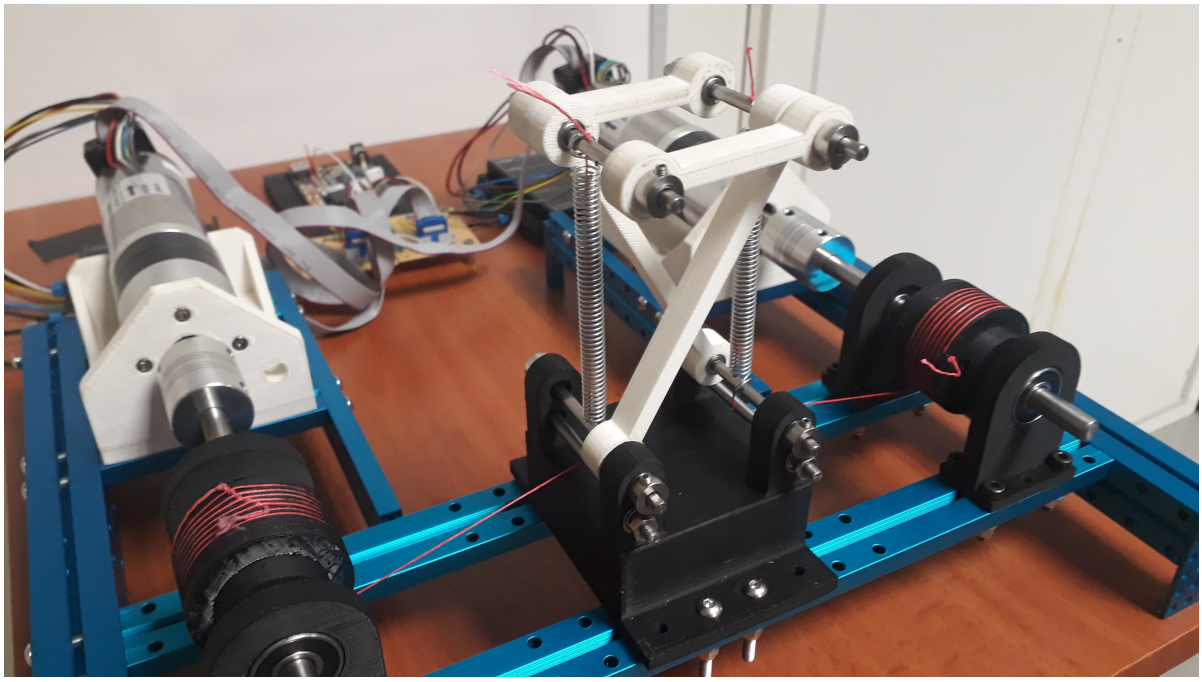

FIGURE 3 – Picture of the prototype

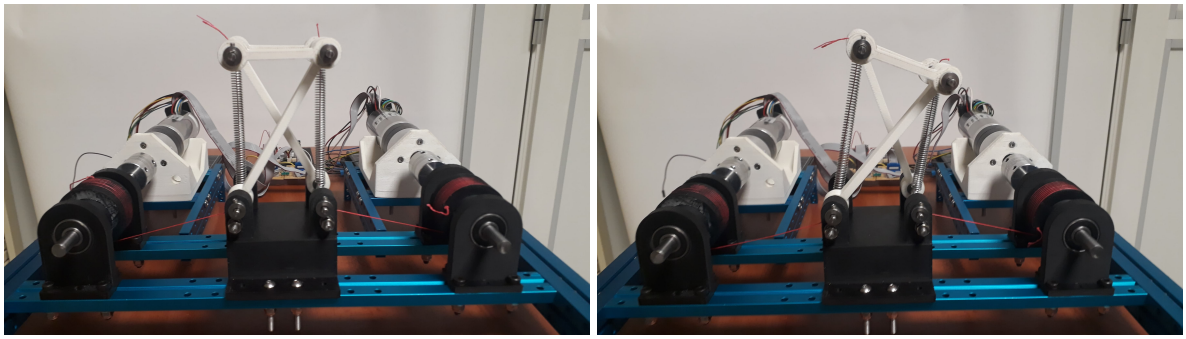

FIGURE 4 – Front view of the rest equilibrium position of the prototype (left) and a given equilibrium position of the prototype with force actuation (right)

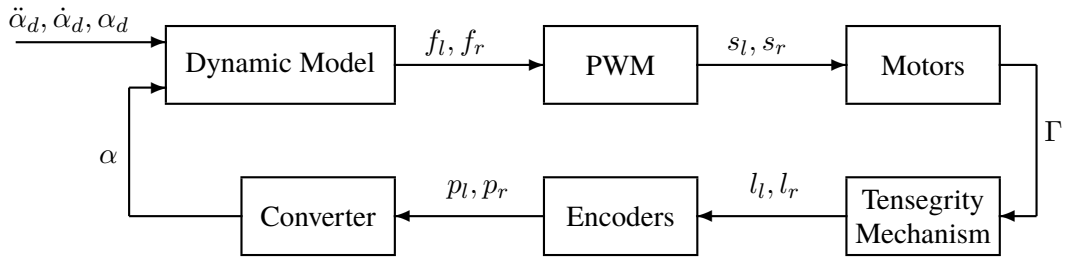

FIGURE 5 – Closed loop

The velocity $\dot{\alpha}$ is also used, thus it must be measured or calculated. These forces are converted in PWM signals s_l, s_r which are given to the motors (thanks to the ESCON controller). Thus, the two motors apply a torque Γ on the drum, which is linked to the torque applied on the mechanism thanks to drum radius and right-hand-side part of equation (1). The lengths l_l, l_r of the two cables are linked to the positions of the motors p_l, p_r, which are the outputs of the encoders. The encoders are directly connected to the beaglebone, with some voltage adaptation. The inclination α of the tensegrity mechanism is deduced from p_l and p_r, the dimensions of the mechanism and the drum.

The algorithm on the Beaglebone is written in C language. The Robot Control Library is used to control the inputs/outputs of the Beaglebone.

4 Conclusion and future work

This article presented the design, the assembly and control of a tensegrity mechanism prototype. After a first modeling of the Snelson X-shape mechanism, a first design has been made. Using 3D-printer and standard parts, a Snelson X-shape has been built. Thanks to cable actuation, forces are applied on the mechanism and modify its equilibrium configuration. The computation of the input forces in made thanks to a dynamic control law. This control law and the PWM signal to motors is provided through both a Beaglebone blue microchip and motor controllers. The real position of the mechanism to be compared with the desired trajectory is computed with motor encoders that measures directly the position of the drum.

This first prototype will be used to validate modeling results on a single mechanism, and the dynamic control law. Future work will be to stack at least two mechanisms, and study different actuation strategies (symmetric or non symmetric cable, side-routed or strut-routed cables) and find the best choice in terms of nature mimicking and performances (workspace, dynamics). This work will be extend to N stacked mechanism, first in 2D, then in 3D.

Références

[1] R. B. Fuller, Tensile-integrity structures, United States Patent 3063521,1962

[2] Motro, R. Tensegrity systems : the state of the art, Int. J. of Space Structures, 7 (2), pp 75–83, 1992

[3] Skelton, R. and de Oliveira, M., Tensegrity Systems. Springer, 2009

[4] S. Levin, The tensegrity-truss as a model for spinal mechanics : biotensegrity, J. of Mechanics in Medicine and Biology, Vol. 2(3), 2002

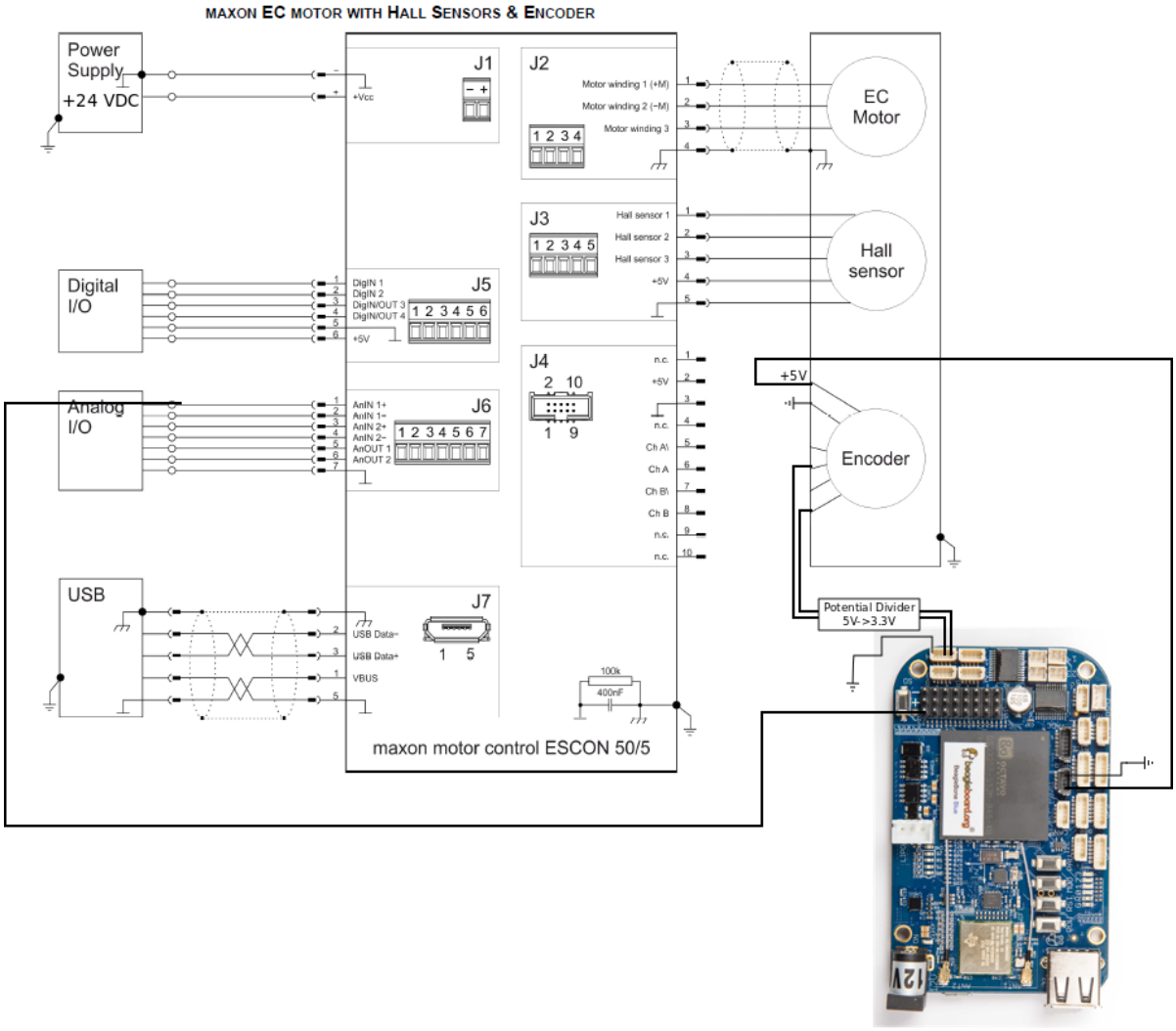

FIGURE 6 – Layout of the interface between the micro-computer, the controller, motor and encoder. This scheme is reproduced for both motors, connecting on the same beaglebone

[5] P. Wenger and D. Chablat, Kinetostatic Analysis and Solution Classification of a Planar Tensegrity Mechanism, proc. 7th. Int. Workshop on Comp. Kinematics, Springer, ISBN 978-3-319-60867-9, pp422-431, 2017.

[6] K. Snelson, 1965, Continuous Tension, Discontinuous Compression Structures, US Patent No. 3,169,611

[7] M. Arsenault and C. M. Gosselin, Kinematic, static and dynamic analysis of a planar 2-dof tensegrity mechanism, Mech. and Mach. Theory, Vol. 41(9), 1072-1089, 2006

[8] C. Crane, J. Bayat, V. Vikas, R. Roberts, Kinematic analysis of a planar tensegrity mechanism with pres-stressed springs, in Advances in Robot Kinematics : analysis and design, pp 419-427, J. Lenarcic and P. Wenger (Eds), Springer (2008)

[9] Q. Boehler, M. Vedrines, S. Abdelaziz, P. Poignet, P. Renaud, Design and evaluation of a novel variable stiffness spherical joint with application to MR-compatible robot design. In Robotics and Automation (ICRA), 2016 IEEE International Conference on (pp. 661-667).

[10] D. Bakker, D. Matsuura, Y. Takeda, J. Herder, Design of an environmentally interactive continuum manipulator, Proc.14th World Congress in Mechanism and Machine Science, IFToMM'2015, Taipei, Taiwan, 2015

[11] J. Rieffel and J.B. Mouret, Adaptive and Resilient Soft Tensegrity Robots, Soft Robotics 2018 Jun 1 ; 5(3) : 318–329.

[12] V. Baum, T. Kaufhold, I. Zeidis, K. Zimmermann, Spherical mobile robot based on a tensegrity structure with curved compressed members. AIM 2016 : 1509-1514.

[13] M Vespignani, J. Friesen, V. SunSpiral, J. Bruce , Design of superball v2, a compliant tensegrity robot for absorbing large impacts. 2018 IEEE/RSJ International Conference on Intelligent Robots and Systems.

[14] A. Van Riesen, M. Furet, C. Chevallereau, P. Wenger, Dynamic Analysis and Control of an Antagonistically Actuated Tensegrity Mechanism, in Romansy 22 – Robot Design, Dynamics and Control, Spinger, ISBN : 978-3-319-78962-0, 2018

[15] M. Furet, A. Van Riesen, C. Chevallereau, P. Wenger, Optimal Design of Tensegrity Mechanisms Used in a Bird Neck Model, in EuCoMeS2018 : Proceedings of the 7th European Conference on Mechanism Science, Springer, ISBN : 978-3-319-98019-95

[16] M. Furet, M. Lett, P. Wenger, Kinematic analysis of planar tensegrity 2-X manipulators, Proc. 16th Internat ional Symposium on Advances in Robot Kinematics, Bologna, Italia, 2018

[17] M. Furet and P. Wenger, Workspace and cuspidality analysis of a 2-X planar manipulator, Proc. 4th IFToMM Symposium on Mechanism Design for Robotics, Udine, Italia, 2018

[18] B. Fasquelle, M. Furet, C. Chevallereau, P. Wenger, Dynamic modeling and control of a tensegrity manipulator mimicking a bird neck, 15th IFToMM World Congress, Krakow, Poland, 2019